DOE/ER/52111-1

Thin Film and Charged Particle Research Laboratory
Report TFCP-03-00

Department of Energy Project
DE-FG02-84ER52111

DEVELOPMENT OF SMALL-BORE, HIGH-CURRENT-DENSITY RAILGUN AS TESTBED FOR STUDY OF PLASMA-MATERIALS INTERACTION

Progress Report for
October 16, 2000 – May 13, 2003

Submitted to:
Dr. T. V. George, SC-52; GTN
Office of Fusion Energy
United States Department of Energy
Germantown, MD 20874-1290

Prepared by
Professor Kyekyoon(Kevin) Kim
Principal Investigator

Thin Film and Charged Particle Research Laboratory
Department of Electrical and Computer Engineering
University of Illinois at Urbana-Champaign
Urbana, Illinois 61801

May 14, 2003

DISCLAIMER

This report was prepared as an account of work sponsored by an agency of the United States Government. Neither the United States Government nor any agency thereof, nor any of their employees, makes any warranty, express or implied, or assumes any legal liability or responsibility for the accuracy, completeness, or usefulness of any information, apparatus, product, or process disclosed, or represents that its use would not infringe privately owned rights. Reference herein to any specific commercial product, process, or service by trade name, trademark, manufacturer, or otherwise does not necessarily constitute or imply its endorsement, recommendation, or favoring by the United States Government or any agency thereof. The views and opinions of authors expressed herein do not necessarily state or reflect those of the United States Government or any agency thereof.

DISCLAIMER

Portions of this document may be illegible in electronic image products. Images are produced from the best available original document.

"Development of Small-Bore, High-Current-Density Railgun as Testbed for Study of Plasma-Materials Interaction"

PI: Kyekyoon (Kevin) Kim
Thin Film and Charged Particle Research Laboratory
Department of Electrical and Computer Engineering
University of Illinois at Urbana-Champaign
May 13, 2003

Abstract

This report summarizes the research progress made during the period October 16, 2002 through May 13, 2003 toward the development of a small-bore railgun with transaugmentation as a testbed for investigating plasma-materials interaction. Since this advanced compact gun can independently control the speed and properties of free-traveling plasma arc, assessing its feasibility as a testbed for studying plasma-materials interaction was warranted. Gun wall erosion and ablation and the resulting impurities that accumulate in the plasma-arc were controlled by separately varying the respective currents in the main rail and the transaugmentation rail, and the gas fill pressure. The impurities were investigated by measuring the variation in the arc velocity along the length of the railgun and the emission spectrum of the arc. The equation of motion of the plasma arc was solved to elucidate the correlation between the physical properties (density and temperature) and dynamical behavior (velocity) of the plasma arc and the erosion property of the railgun wall materials. Due to the limited funding ($40K for the entire period) the work performed could not be extensive, however, it has generated ample evidence indicating that the transaugmented compact railgun may very well serve as a powerful tool for studying plasma-materials interaction.

DOE Patent Clearance Granted
MP Dvorscak 6·19·03
Mark P. Dvorscak Date
(630) 252-2393
E-mail: mark.dvorscak@ch.doe.gov
Office of Intellectual Property Law
DOE Chicago Operations Office

OBJECTIVES

The principal objectives of this work were two-fold: to operate a small-bore railgun with transaugmentation at high currents to induce wall erosion/ablation, identify/study the resulting impurities in the free-traveling plasma-arc, and, in doing so, develop the advanced railgun as a testbed for studying plasma-materials interaction.

MOTIVATION

An advanced compact railgun system exists at the UIUC which, due to its small bore and unique transaugmentation features, is particularly suited to producing free-traveling high-current-density plasma-arcs with controlled properties under various operating conditions. Since these arcs give rise to controlled ablation of gun wall material, the railgun system provides a cost-effective means of producing/studying impurities in the plasma-arcs and thereby testing/developing schemes for the study of plasma-materials interaction.

SUMMARY

This report summarizes the research progress made during the period October 16, 2000 through May 13, 2003 toward developing a compact system by which to perform an in-depth study of the impurities that accumulate in a free-traveling high-current-density plasma inside a small-bore railgun and, by making use of the transaugmentation scheme, to develop a comprehensive testbed for the study of plasma-materials interaction. Gun wall erosion and the resulting impurities that accumulate in the plasma-arc were controlled and studied by separately varying the respective currents in the main rail and the transaugmentation rail and the gas fill pressure, and by measuring the arc velocity profile and plasma emission spectrum. The major departure between the present work and the work performed during the previous years was that the original two-stage gun consisting of the first-stage gas-gun pellet pre-accelerator/injector and the second-stage railgun booster accelerator was modified into a single-stage railgun so that it may create and accelerate free-traveling plasma arc under a variety of controlled operating conditions. Much of the principal instrumentation, however, remained intact as far as observation of the plasma-arc motion was concerned. The tools for spectroscopic measurements were added to measure rail erosion resulting from the interaction between the plasma and the gun wall materials. Another element added to the previous work was the development of detailed analytic tools with which to analyze the gun erosion so that the mechnisms of the plasma-gun wall interaction may be comprehensively elucidated. The specific tasks undertaken during the current research period and the results therefrom may be summarized as follows.

1. A compact small-bore railgun system with a unique transaugmentation scheme designed to generate and study free-traveling plasma arcs with varying plasma properties and velocities was extensively studied. This system was furnished with the necessary

controls and diagnostics. The current-pulse-forming network was upgraded to achieve the highest current density possible with the existing power supply and the capacitor bank.

2. The free-arc experiments were performed using the main railgun current carried by the free arc and the transaugmentation rail current designed to accelerate or decelerate the plasma-arc motion. To enable free-arc experiments electrical discharge was generated at the breech of the railgun using a unique arc-initiation scheme developed at the UIUC. This plasma arc was subsequently accelerated along the length of the railgun using two independent current pulses with controlled amplitudes, ramping rated, and durations. Depending on the control parameters the plasma arc could be made to be arrested inside the railgun bore, or shoot out at the gun muzzle into a probing chamber. The operating parameters varied for this study were the initial fill pressure of the hydrogen gas, the peak rail currents, and the current pulse profiles.

3. The change in the plasma arc velocity inside the gun bore was measured using an array of B-dot probes installed over the length of the railgun. This velocity data, combined with the spectroscopic data from the plasma emission measurement and an analytical model we developed, gave us information on the amount of gun erosion and ablation caused by the plasma arc and provided a guideline with which to estimate the ablation thresholds and ablation rates of the materials comprising the gun wall.

4. Work was undertaken to study the impurities in the plasma arc in relation to the materials comprising the railgun wall and the operating parameters. Spectroscopic measurement was employed as the main diagnostic tool to study the impurities. This impurity study covered a wide range of operating parameters and the results were subjected to an analysis to correlate the impurities with the wall material and operating parameters of the railgun. These operating parameters included the initial hydrogen gas pressure, the peak rail currents, and the current profiles, particularly, the ramping speeds.

5. The equation of motion of the plasma-arc was solved for various cases to elucidate the correlation between the observed velocity profiles of the plasma-arc and the possible

physical processes responsible for them. This procedure should allow one to determine the material properties pertaining to ablation and also provide a guideline for minimizing it.

RESULTS TO DATE AND DISCUSSION

The results obtained during the course of the present investigation may be categorized and discussed as follows. The results in sections 1 through 4 are a summary of those obtained previously. The results in section 5 are a summary of more recent work.

1. Plasma-Arc Velocity vs. Gas Pressure and Bank Voltage

The velocity profiles of the traveling plasma-arc were measured at various initial gas fill pressures using an array of B-dot probes. Figure 1 shows a plot of plasma-arc velocities along the length of the railgun obtained at a capacitor bank voltage of 6 kV for five different fill gas pressures from 10 torr to 50 torr. At 6kV the highest free-arc velocity is shown to be around 16 km/s which is achieved at 10 torr. Figure 2 contains a plot of plasma velocity vs. capacitor bank voltage at different gas fill pressures. General observation of these three figures reveals that the plasma-arc initially accelerates attaining a maximum velocity somewhere before the midpoint of the railgun, but after that it decelerates toward the gun muzzle and that the velocity decreases with increasing gas fill pressure and increases with increasing capacitor bank voltage. This latter observation is not surprising since higher the gas fill pressure, the heavier the plasma-arc mass making it more difficult for the arc to get accelerated and since with higher power input, the plasma arc, in general, should accelerate more. The fact that the arc velocity first increases, but starts to decrease midway in the gun bore, however, was not expected. It indicates that effects such as inertial drag and viscous drag that cause plasma deceleration are making contributions. Since these effects result from gun wall erosion and ablation subsequently depositing impurities in the plasma-arc, to alleviate such effects one must reduce the amount of wall material erosion and ablation. This may be achieved either by a judicious choice of the wall material so that it may be ablation-resistant or by implementing a current pulse shaping network that minimizes heating of

the gun wall. A detailed analysis addressing this particular issue will be presented later. The temporal profiles of the railgun current corresponding to different capacitor bank voltages are plotted in Figure 3.

2. Plasma Gas Mass vs. Ratio of Railgun Current and Plasma-Arc Velocity (I/v)

Although a more detailed analysis will be presented later, in general, in the analysis of free-arc data, plots of effective plasma mass (m_g) as a function of I/v provide information concerning the relative armature mass, ablation coefficients, and degrees of ablation at various operating parameters. More specifically, the following observations hold true:

- Closely spaced I/v values for a given m_g indicate negligible ablation.
- For a given m_g, lower I/v values correspond to lower plasma-arc masses and lower ablation coefficients of the wall material.
- An increase in I/v with increasing m_g provides a means of estimating the armature mass.

The above aspects are evident in Fig. 4 through Fig. 7 where gas mass is plotted against the ratio between the rail current and the plasma-arc velocity (I/v). Figure 4 is from hydrogen plasma arc acceleration experiment using a 1.2m gun consisting of three different insulating sidewall materials, lexan, mullite and perforated lexan. For each given value of the gas mass, the spread in the I/v value increases as one moves from mullite, to perforated lexan, and then to lexan, indicating increasing amount of wall ablation. The reason is that mullite, a ceramic material, has an ablation threshold much higher than that of lexan. The lexan wall with perforation can remove, from inside the gun bore, the ablation debris coming off the wall, thus reducing the mass of the plasma arc, which, in turn, decrease the inertial and viscous drag, and, subsequently, a spread in the I/v value since higher arc velocity is possible at a given current. Similar results obtained with a helium plasma-arc are presented in Fig. 5. The sidewall materials used for the 2m-railgun studies (Fig. 6 and 7) were lexan and mullite. Perforated lexan was not employed. These figures clearly indicate that the gun made with mullite wall

produces much less ablation which is indicated by the much smaller spreads in the I/v values for mullite as compared to those for lexan.

3. Plasma Emission Spectra and Identification of Ablation Sources

Work was undertaken to study the impurities in the plasma arc in relation to the materials comprising the railgun wall and the operating parameters. Spectroscopic measurement was employed as the main diagnostic tool to study the impurities. This impurity study covered a wide range of operating parameters and the results were subjected to qualitative analysis to correlate the impurities with the wall materials and the operating parameters of the railgun. These operating parameters included the initial hydrogen gas pressure and the peak rail current. The typical results of the spectroscopic study performed to date are presented in Figures 8 through 14. Figure 8 shows the emission spectrum of a hydrogen plasma obtained at 6 kV and 10 torr. These spectroscopic data indicate that the plasma arc contains debris from both the sidewall which consists of G-10 and the rail electrode which is made out of Cu and that the amount of gun wall debris in the plasma-arc increases with increasing rail current. Due to an overlap between the emission lines of G-10 and Cu, however, quantitative statement could not be made as to which of the two gun wall materials, G-10 and Cu, ablated more with an increase in the rail current. Figures 9 through 13 show plots of various line emission intensities from the plasma arc vs. capacitor bank voltage, for five different initial fill gas pressures. All except Fig. 11 show an emission spectrum characteristic of the sidewall material, G-10. The 408-nm line emission shown in Fig. 11 is tied to both the G-10 sidewall and the Cu rail electrode. All of these spectra show increasing luminescence intensities with increasing capacitor bank voltage and decreasing fill gas pressure indicating that the emission intensity increases with an increase in the energy of the individual particles in the plasma. The spectroscopic data contained in Figs. 9 through 13 are rearranged in Fig. 14 against the principal emission line of G-10 which is 394nm. This plot clearly indicates that all emission lines behave essentially the same way and that the line containing the emission from Cu is slightly lower than the other emission lines due to the fact that the ablation threshold of Cu is higher than that of G-10. Further analysis of this data is needed to extract more useful information that may

facilitate development of possible schemes for preventing erosion and ablation of the gun wall material.

4. ANALYSIS OF FREE-ARC DATA

The data included in Figures 1 through 14 presented evidence that heating by the high-current-density plasma arc results in erosion and ablation of the gun wall material and that as this wall material debris accumulates in the plasma arc, it eventually causes the arc to decelerate in all of the cases studied. To further elucidate the causes for the plasma-arc slowdown, the equation of motion of the free arc was analyzed. As the arc travels inside the gun bore, it causes pulsed heating of the gun wall surface which brings about either melting or vaporization of the surface when the heat flux exceeds the ablation threshold of the gun wall material.

The detailed equation of motion of the free arc and its solutions for the cases of current interest are presented in the following section. One of the most significant results of this analysis is that a physically meaningful closed-form solution is found for a realistic situation where mass of the plasma arc changes with time, namely, a situation where inertial drag cannot be ignored. Although it takes some computational effort to use the solution and determine the quantities of our interest, such as the ablation coefficient and the actual free-act velocity profile, there is no question that in time an efficient numerical code can be developed to make it a routine exercise. It is, therefore, safely concluded that by analyzing the solution and comparing it with the experimental results one may determine and predict the response of a given material to a plasma once its relevant parameters, such as the temperature, density, and species, are specified. This is very significant since it opens up a door for a small-bore railgun operating at high currents to be used as a test stand to produce and study material ablation. Together with the closed-form solution to the equation of motion of the free arc, the UIUC compact railgun may, therefore, serve as a convenient tool for testing and developing schemes/materials with which to eliminate material erosion and ablation .

The excellent opportunity to utilize a compact railgun to conveniently test plasma-facing materials may be further expanded by adding an augmentation rail to the existing railgun system as illustrated by Figure 15. The significant benefit of using an

augmentation rail is that the acceleration force on the plasma arc can be controlled by varying the magnitude and the direction of the current in the augmentation rail as indicated by the expression for the Lorentz force presented in Figure 15. In other words, by using a negative current of appropriate magnitude in the augmentation rail one may, in principle, stop the motion of the free arc, thus increasing both the residence time of the arc and the amount of ablation of the gun wall material at a given point of the gun bore. This unique capability of an augmented railgun tremendously enhances its usefulness as a test stand for the plasma-facing materials.

5. SIMULATIONS

The goal of the simulation was to measure the ablation parameters. Ablation parameters serve to quantify the loss mechanism or performance of the railgun operation. In order to estimate these parameters, it is a must to introduce the concepts and models regarding the railgun ablation.

5.1 Ablation Models

The physical process occurring in the arc of a railgun is extremely complex, so some simplifications are necessary. A complete description would require a three-dimensional transient solution of the conservation of mass, energy, momentum, Maxwell's equations, and several auxiliary relations. The approach used here is to neglect spatial variations of arc properties so that values of arc temperature, etc. are regarded as average values. The effect of this simplification appears to have a minor effect on the calculation of the mass of the arc.

Thermal ablation is the result of an intense heat flux from the plasma armature incident upon the bore walls. The small heat capacity of plasma armature makes the exchange of energy between the plasma and the walls nearly instantaneous. The heat flux from the armature can be as high as several MW per square cube meter in a small bore railgun.

There are two categories of perceptions about ablation: (i) radiation dominant and (ii) radiation and convection combined.

The analysis of plasma armature in EM launcher has revealed behavior that suggests the ablation of the railgun bore constituents and subsequent ionization of them into the plasma armature. A simple worst-case model for predicting the material mass removed from the bore, and consequently added to the armature, is

$$\frac{dm_a}{dt} = \alpha I V_a \quad , \tag{5.1}$$

where m_a is armature mass,

I is armature current,

V_a is arc voltage, and

α is ablation constant.

The ablation constant α is material dependent and can be approximated by calculating the energy per gram required to ionize it. Since the dominant factor in determining the ablation constant is the average atomic weight of the material, a close approximation can be found using the following relationship

$$\alpha = \frac{3n}{4} g \quad , \tag{5.2}$$

where n is the average atomic weight of the bore materials.

Ablation affects the performance of a plasma armature railgun in at least two ways: The first in the increase in the overall launch package mass which may be determined, and the second being the force associated with the change in the launch package mass while moving at velocity, v, which can be determined by

$$F_a = v\frac{dm_a}{dt} = \alpha I V_a v \quad . \tag{5.3}$$

The conditions for operating a railgun without ablation are straightforward. To first order the moving plasma armature can be modeled as delivering a square wave heat pulse to the bore walls. Solving Fourier's equation for heat conduction and rearranging terms gives

$$qt^{\frac{1}{2}} = 0.5(T_f - T_i)\sqrt{\pi \rho c_v k} \quad , \tag{5.4}$$

where q is incident heat flux,

t is exposure time,

T_f is final wall surface temperature,

T_i is initial wall surface temperature,

ρ is density of the wall,

c_v is specific heat at constant volume, and

k is thermal conductivity.

Using the vaporization temperature T_v of the wall material for the final temperature in equation (5.4) gives the highest allowable heating the wall material can withstand before ablating. With $T_f = T_v$, the right hand side of the same equation q can be regarded as a figure of merit for the bore materials, sometimes referred to as the f-value. The higher the f-value, the more resistant the material to ablation.

The f-value for common rail materials is significantly higher than those for any of the presently available insulators, which therefore sets the limits for ablation-free operation. The f-values for currently available sintered ceramic materials are an order of magnitude better than for plastic railgun insulators. Only high thermal conductivity ceramic makes ablation-free operation possible in a practical railgun.

Because heat transfer from the plasma to the wall is nearly instantaneous, the power radiated to the wall is equal to the Joule heating, IV_a. Assuming the plasma length l and

velocity v do not change during the period of exposure, equation (5.4) can be rewritten as

$$\frac{I_r V}{4w\sqrt{lv}} = 0.5(T_f - T_i)\sqrt{\pi\rho c_v k} \equiv f\text{-}value \quad . \tag{5.5}$$

where w is the bore width of the square bore railgun assumed in this model.

This inequality defines the conditions for operating a railgun below the ablation threshold. A number of approaches can be used to satisfy the condition of equation (5.5), i.e.

1) Use insulators with high f -value or low ablation;
2) Minimize bore power, $I V_a$ or use transaugmentation;
3) Operate the launcher with a high initial velocity;
4) Use perforated railgun side walls;

Unlike the radiation dominant models, some evaluations indicate that the major effect limiting the achievable velocity results from ablation caused by turbulent convective heat transfer at the bore of the railgun. This contrasts with the more commonly held view that radiation from the plasma is the major source of ablation.

The influence of ablation, whether caused by radiation or convection, is that a fraction of the ablated wall material is swept up into the plasma and heated and accelerated to the plasma velocity. The increased plasma mass and the energy lost in the acceleration process limit the railgun performance. The cold ablated material that is not entrained in the armature is a concern if it causes damage to the bore surfaces. More importantly, if it is heated by a secondary arc and becomes conducting, it may divert current from the primary arc, thereby reducing the accelerating force on the projectile.

A far more important effect driven by the parasitic power dissipation is the radiative and convective heat transfer from the plasma armature to the rail and insulator surfaces of the bore through the boundary layer at the wall. This heat transfer results in ablation of

the inner wall surfaces. A fraction of the ablated material is entrained in the armature plasma and heated to the plasma temperature. This entrained mass moves with the projectile at velocity v. This ablation process leads to parasitic loss terms generating work against the driving magnetic force: the mass added to the armature by ablation and its ablation rate produces a decelerating force and a drag force on the projectile.

In this context, the ablation rate is modified to be

$$\frac{dm_a}{dt} = \frac{f_e\left[\dot{R} + \dot{H}\right]}{\Delta h_w} , \tag{5.6}$$

where f_e is the entrainment factor, and Δh_w is the difference in enthalpy between the cold wall and the inner surface of the boundary layer, the so-called enthalpy of ablation.

The radiation rate impingent on the walls, $\dot{R}$, is given by

$$\dot{R} = \frac{4m_a}{D\rho_0}\sigma T_e^4 , \tag{5.7}$$

where σ is the Stefan-Boltzman constant, and T_e is the effective temperature of the plasma seen by the cold wall through the boundary layer.

A full determination of T_e requires a three-dimensional, time dependent magnetic and hydrodynamic-radiation transport-turbulent boundary layer calculation. Calculations of T_e for conditions similar to these found in hypervelocity railgun plasmas suggest that T_e is typically less the 1eV (11,604K).

The second term in the ablation rate equation, $\dot{H}$, represents the turbulent convective heat transfer to the walls through the boundary layer and is proportional to the turbulent heat transfer coefficient, C_H, $\dot{H}$ is expressed as

$$\dot{H} = \left[4 C_H m_a \frac{v}{D} \left(E + \frac{P}{\rho_0} + \frac{1}{2} v^2 - \Delta h_w \right) \right] . \tag{5.8}$$

For the condition found in hypervelocity railgun plasma, we can let $C_H = C_D$.

Unfortunately, from the point of view of being predictive equations, these equations contain the three heuristic parameters, the drag coefficient C_D, the entrainment factor f_e and the enthalpy difference between the cold wall and the inner edge of the boundary layer, the so-called ablation enthalpy, Δh_w. In this work C_D is taken as 0.0032 (between 0.0015 and 0.006) and Δh_w is taken as 100 Hp/(MJ/kg).

The entrainment factor, f_e, is the least known of the three heuristic parameters. It quantifies the fact that not all of the material ablated from the walls is heated to the plasma temperature and accelerated with the armature. A related critical question is what happens to the fraction of ablated material (1- f_e), which is not entrained in the armature. If that mass were lost to the back of the moving armature-projectile system without any further consequence, it would only matter if it caused damage to the bore. The real effect is potentially much more serious. The ablated mass that is not entrained in the plasma armature traveling with the projectile is very cold compared to the entrained mass. A secondary arc that could reduce the acceleration of the projectile could heat it.

5.2 Inputs and Outputs

Deciding a practical range for the power source is a top priority for simulation since a variety of insulating materials with distinctly different ablation parameters. Next, we will make analyses and come to conclusions allowing us to determine high current values.

Let us consider the Lorentz force $F_l = 2\times 9.81 rBI$ with $B = \frac{\mu_0}{\pi L} I$ in a simple cylindrical railgun. Then maximum terminal velocity $\hat{v}$ given in the non-ablation region, based on the fact that the velocity reaches this value rapidly and remains constant for a substantial period of time, approximately leads to the average armature velocity in term of rail current as

$$\bar{v} = \left(\sqrt{\frac{2\times 9.81\mu_0}{\pi L C_d (m_0 + m_g)}}\right) rI , \tag{5.9}$$

which is obviously proportional to the rail current I. This indicates that as the rail current increases, the average velocity will continue to rise linearly until the ablation arises when the arc then moves below the ablation threshold velocity

$$\tilde{v} = \frac{V^2}{(2\pi r f)^2 l} I^2 . \tag{5.10}$$

The current corresponding to the intersection of these two types of velocity curves (see Figure 5.1) is the ablation threshold current whose magnitude can be calculated using the following formula

$$\tilde{I} = \frac{4\pi r^3 f^2 l}{V^2} \sqrt{\frac{2\times 9.81\pi\mu_0}{L C_d (m_0 + m_g)}} . \tag{5.11}$$

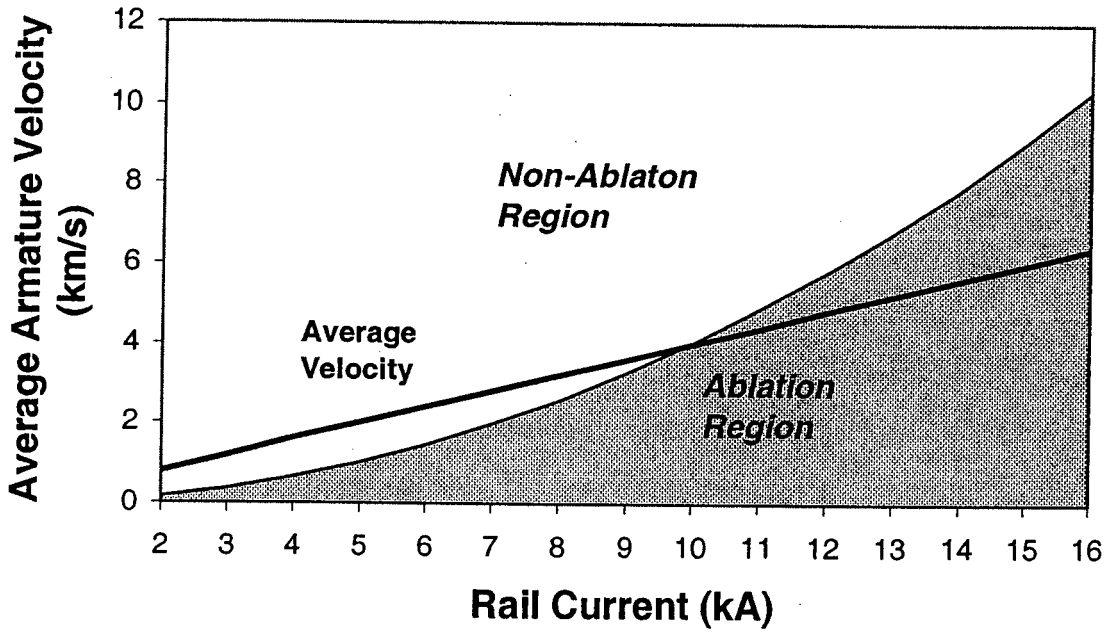

Figure 5.1 The threshold current for ablation

The ablation threshold current defines the minimum quantity of rail current required to ablate the material. It varies widely among the candidate insulators. Lexan, for example, has a very low ablation threshold current of less than 100A while Graphite and Diamond have ablation threshold current of as high as several thousand kiloamperes, as shown in the third column of Table 5.1. Undoubtedly, such significant differences give rise to difficulties in designing a test stand for practical use. A practical test stand needs to operate within a reasonable rail current range for insulators of various ablation thresholds. This presents one of the key challenges in design process.

In principle, if the insulator's surface is exposed to thermal flux of sufficient intensity and duration, then ablation occurs. As cited in equation (5.5), the heat loading is a product of heat flux and exposure time. For example, for materials with high ablation thresholds, the intensity of the heat flux is relatively small, so the exposure time needs to be long. At the other extreme, for materials with low ablation thresholds, the intensity of the heat flux is relatively high, so the exposure time needs to be short. In summary, the exposure time needs to be controllable.

Varying rail current seems to be a means of controlling the exposure time. However, this approach will complicate the control process because rail current is related both to heat flux directly and to exposure time indirectly. As an alternative, exposure time can be controlled independently by using backfill gas and augmentation. The armature velocity can be adjusted by changing the species and pressure of the backfill gas. Unlike conventional railguns, an augmented railgun can strengthen or weaken the driving force on the armature without affecting the heat flux level. With the augmented rail current, the Lorentz force becomes

$$F_l = \frac{2\times 9.81\mu_0 r}{\pi} I_r \left(\frac{I_r}{L_r} + \frac{I_a}{L_a}\right) . \tag{5.13}$$

Consequently, we can find the augmented current for any desired rail current. In fact, augmentation significantly and efficiently controls the exposure time. In practice, a

combined approach will be used. For instance, for the higher ablation threshold insulator, a denser gas at higher pressure and negative augmented current will increase the exposure duration, making the material prone to ablate. This combined technique provides greater flexibility in determining the operating parameters used as technical specifications for simulation, as listed in Table 5.1 below.

In addition to rail current, a couple of input variables are required for the simulation. For example, gas type, gas pressure, railgun geometry and heat parameters of insulator materials are quite crucial for the model implementation. In details, the basic inputs and outputs are listed in following Table 5.2.

Table 5.1 Operating parameters for selected insulators in 2m railgun

Insulator Materials	Ablation Threshold ($MWs^{0.5}/m^2$)	Critical Current [kA]	Rail Current (Augmented) [kA]	Gas Pressure [torr]/Type	Armature Heat Flux [GW/m^2]	Exposure Time [μs]	Minimum Pulse Width [μs]
Lexan	0.223	0.083	0.365 (+10.0)	0.1 /He	0.2	0.9	96
SiO_2	2.40	9.6	9.6 (0)	0.1 /He	4.9	0.3	48
Mullite	4.09	12.3	12.3 (0)	10 /He	6.2	0.4	40
Si_3N_4	13.8	18.2	18.2 (0)	100 /Air	9.3	2.2	232
Al_2O_3	16.4	25.7	20.0 (-15.0)	100 /Air	10.4	2.6	268
SiC	31.0	33.5	25.0 (-20.0)	760 /Air	13.0	5.5	572
Graphite	73.0	185.5	25.0 (-40.0)	760 /Air	13.0	7.5	784
Diamond	210	1535	30.0 (-50.0)	760 /Air	15.6	182.0	18988

Table 5.2 The basic inputs and outputs for simulations

INPUTS	OUTPUTS
Rail current [KA]	Armature velocity [m/s]
Muzzle voltage [V]	Armature mass [μ g]
Backfill gas type	Ablation rate [kg/MJ]
Gas pressure[torr]	Ablation threshold [MWs^0.5/m2]
Railgun length [m]	Bore wall temperature [K]
Drag coefficient [kg/J]	Exit time [μ s]
Initial Velocity [m/s]	
Initial wall temperature [K]	
Insulator specific heat [J/kg-K]	
Insulator thermal conductivity [W/m-K]	
Insulator density [kg/m3] * 10e3	
Time interval [μ s]	
Number of time step	
Simulation number	

Table 5.3 The comparison of published and simulated ablation parameters

(a) Ablation Rate

Insulator Materials	Density [kg/ m^2] *10e3	Thermal Conductivity [W/m-K]	Specific Heat [J/kg-K]	Published Ablation Rate (kg /MJ)	Simulated Ablation Rate (kg /MJ)
Lexan	1.2	0.3	1200	4-8(p)	7.15
G-10	1.9	0.73	1570	6.7(p)	5.83
Mullite	2.3	4.1	848	~5.6(p)	6.48

(b) Ablation Threshold

Insulator Materials	Density [kg/ m^2] *10e3	Thermal Conductivity [W/m-K]	Specific Heat [J/kg-K]	Published Ablation Threshold ($MWs^{0.5}/m^2$)	Simulated Ablation Threshold ($MWs^{0.5}/m^2$)
Mullite	2.3	4.1	848	4.094(r)	3.823
Al_2O_3	3.96	39.0	880	20.6(p)	22.74
Lexan	1.2	0.3	1200	0.227(r)	0.411
SiC	3.1	126.0	669	35.8(p)	38.39
Si_3N_4	3.28	27.6	810	15.5(p)	13.46

Remarks: (p) denotes source from Parker; (r) denotes source from Rosenwasser

These analysis and discussions are stated as follows:

1) The results are comparable with values published by other researchers. The error percentage between the simulated and published figures is within a reasonable range, most of them are smaller than 15 % and some of them are even less then 10%. For instance, the simulated ablation thresholds of Lexan and SiC are only 6.6% and 7.2%, respectively, distinct from the published numbers. In terms of absolute magnitude, the Lexan has only 0.271 less and Mullite has only 0.184 more for ablation threshold. The ablation rate of Lexan falls into Parker's prediction, and majority of the simulated results are close around the other author's estimations. This indicates that the simulation can achieve a desired level and results are reasonable and as expected. The proposed simulation methods prove feasible and successful.

2) The accuracy of the parameter estimation is controllable with simulation numbers. This is attributed to controllable error bounds of the quasi-Monte Carlo method. With applications of such methods, the simulation time is saved to a greatest degree compared to other simulation methods. The random number generator is efficient enough to reduce the computational burdens of the stochastic simulation. Faster convergence and higher accuracy are the salient features of the simulation.

SUMMARY AND CONCLUDING REMARKS

In this report we described the research progress made during the period of October 16, 2000 through May 13, 2003 toward developing a scheme by which to study the interaction between the free-traveling plasma arc with a variety of properties and the gun wall materials. A small-bore railgun with the transaugmentation capability was used and operated at high currents. This allowed us to generate and study a free-traveling high-current-density hydrogen plasma-arc and, in particular, the impurities in it resulting from erosion and ablation of the gun wall material. The amount of impurities was controlled by separately varying the currents in the main rail and the augmentation rail and the gas fill pressure. These impurities were then studied by measuring the change in the arc velocity along the length of the railgun and in the plasma emission spectrum. The equation of motion of the free-arc was solved for two different cases to elucidate the physical processes responsible for the observed change in the arc velocity. Use of an augmentation rail was proved to be effective in controlling the arc velocity at a given plasma current, to the point that, if necessary, the arc could be arrested to stop completely. As a result, it was possible to control the amount of the resulting erosion and ablation of the gun wall material. Because of this unique capability it is concluded that our advanced raillgun system together with the augmentation scheme offers a powerful, inexpensive testbed that facilitates comprehensive testing and development of new plasma-facing materials that are resistant to ablation.

Plasma Velocity vs. Distance from Start (6KV)

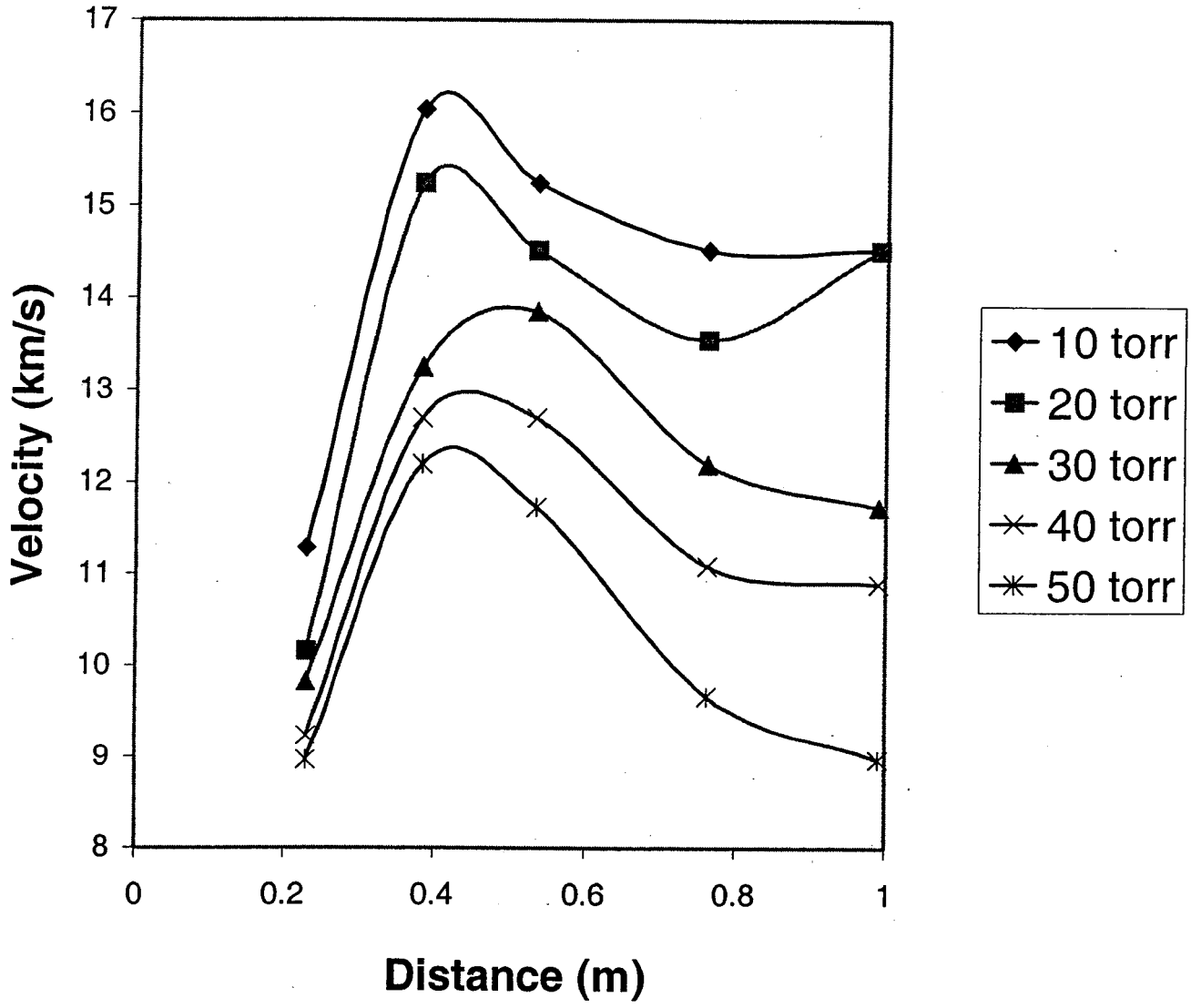

Fig. 1

Plasma Velocity vs. Bank Voltage at Different Gas Pressures

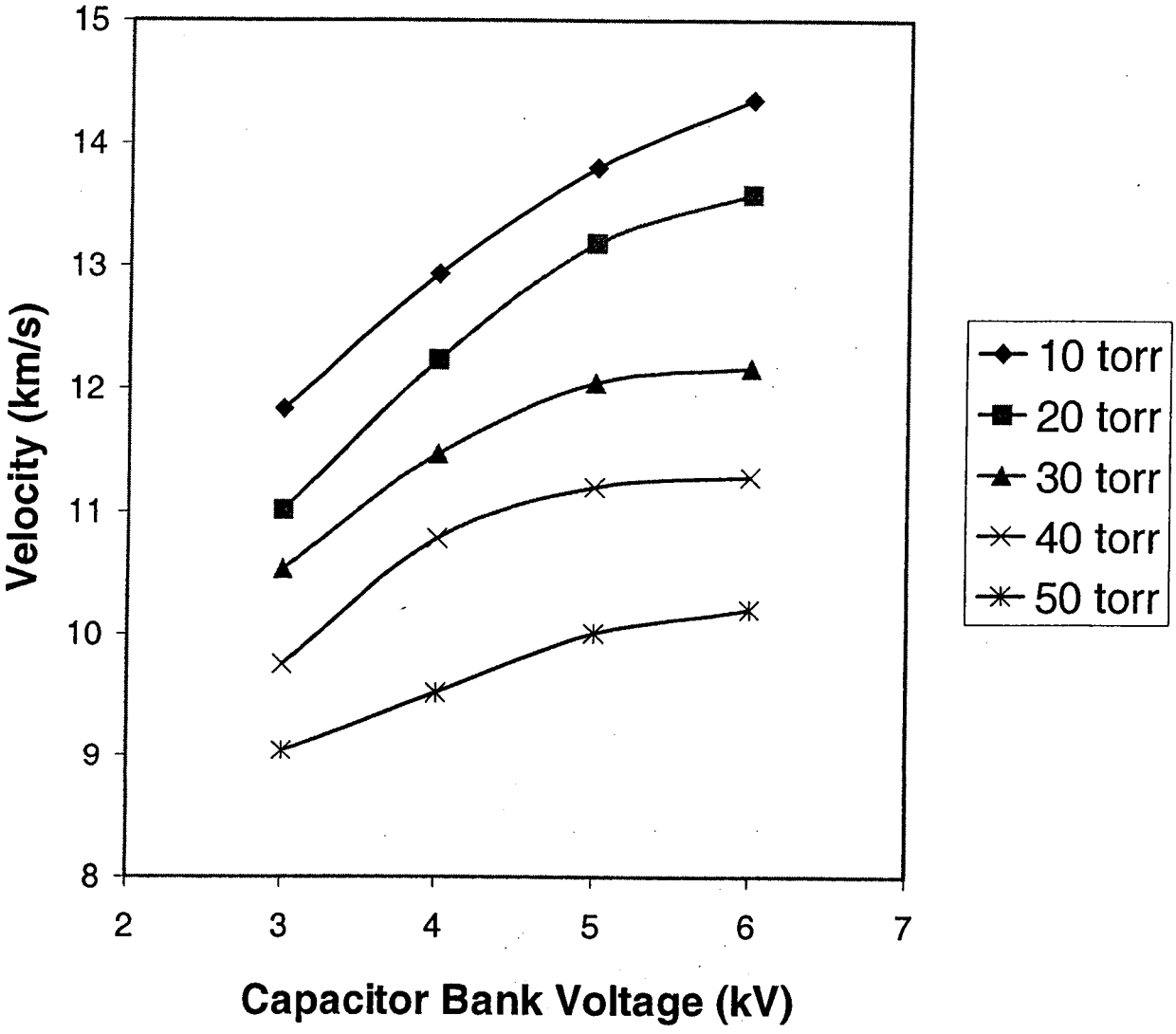

Fig. 2

Railgun Current Pulse

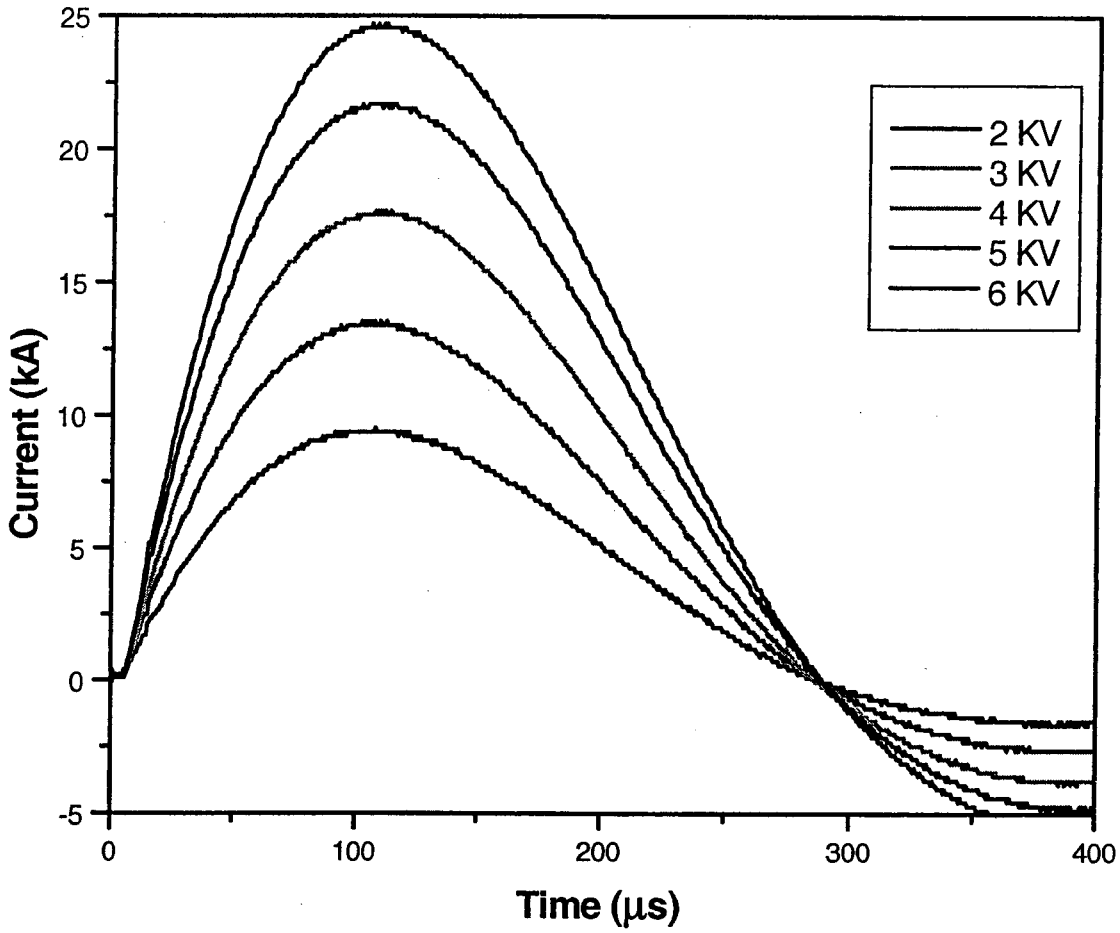

Fig. 3

Hydrogen Gas Mass vs. I/v on 1.2m Gun

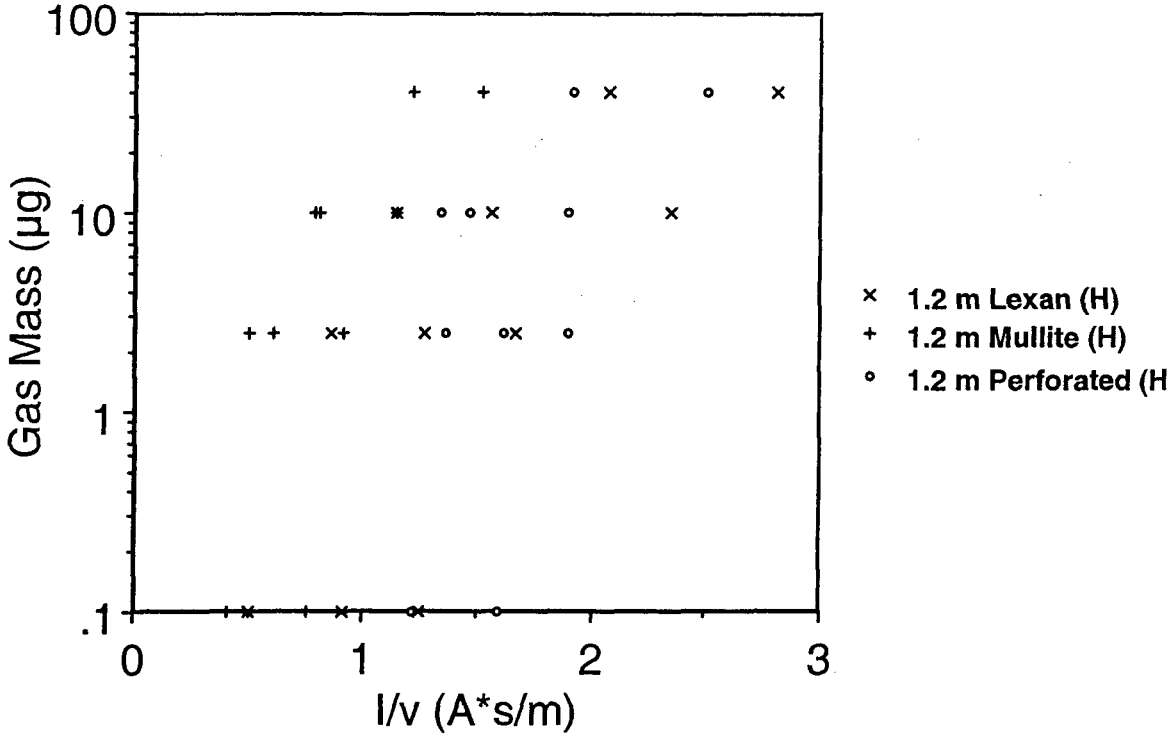

Hydrogen gas mass vs. I/v on 1.2 m gun

Fig. 4

Helium Gas Mass vs. I/v on 1.2m Gun

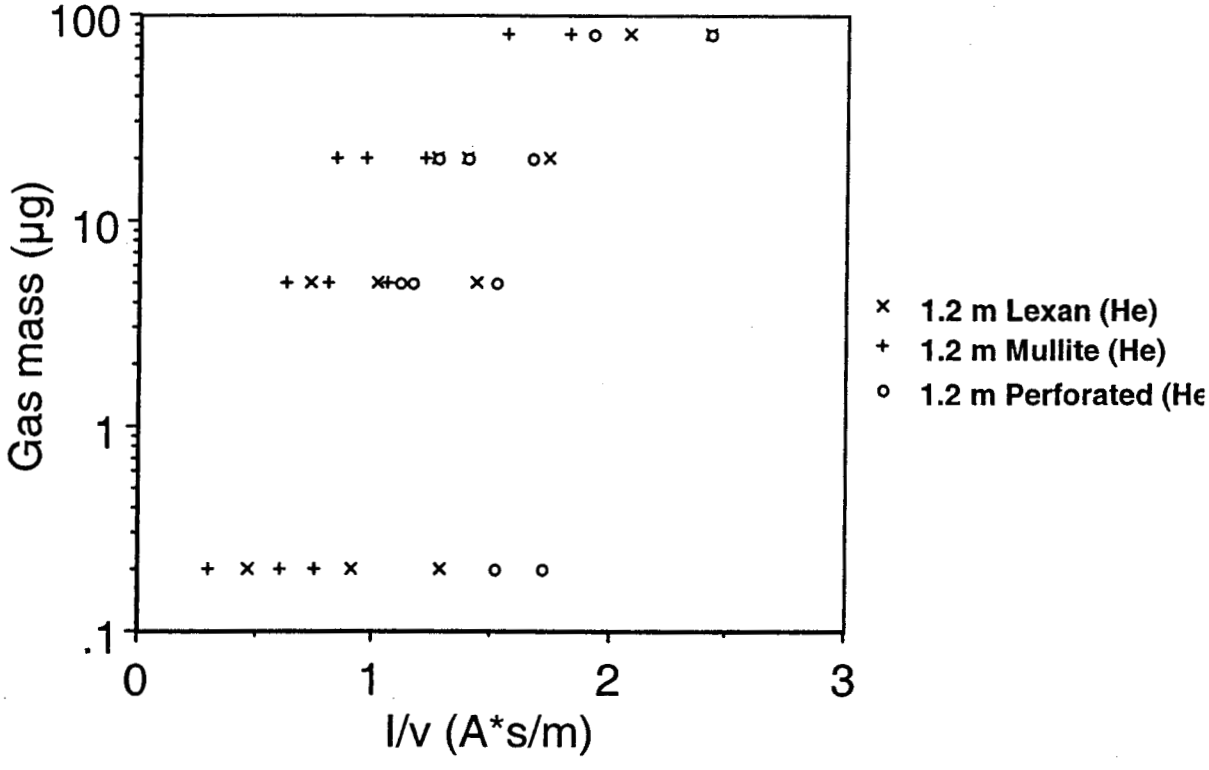

Helium gas mass vs. I/v on 1.2 m gun

Fig. 5

Hydrogen Gas Mass vs. I/v on 2m Gun

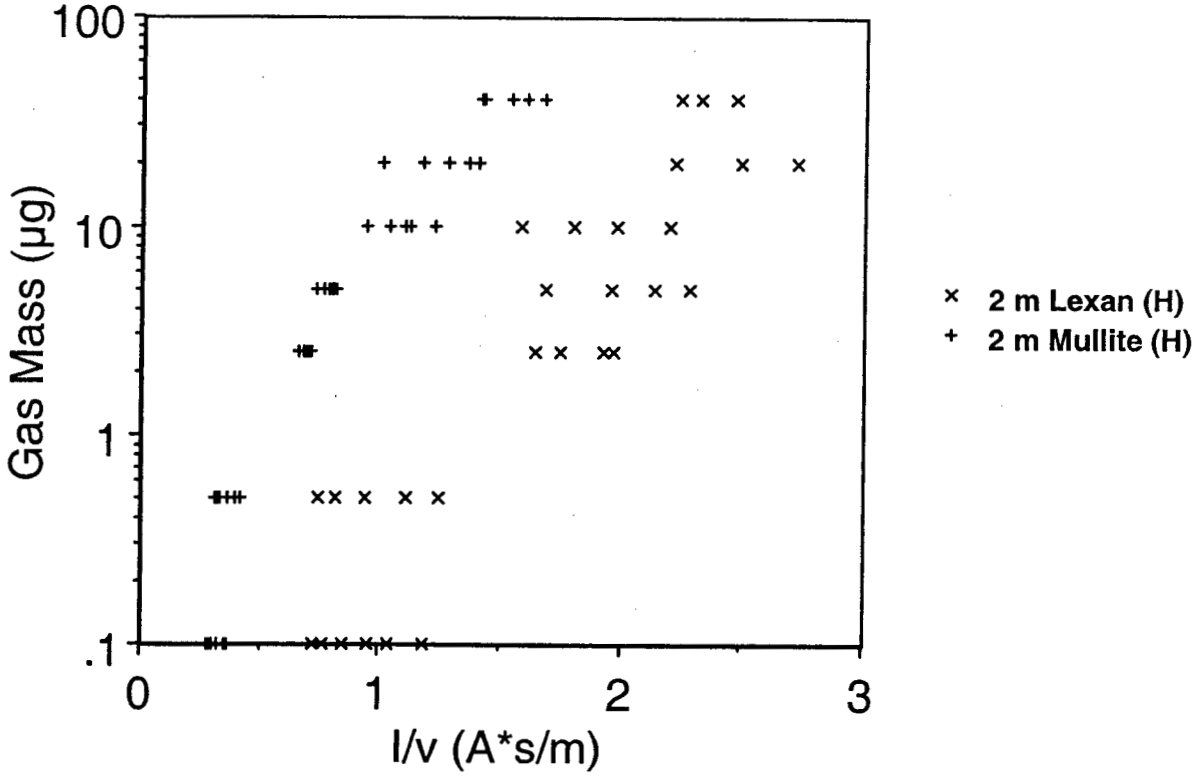

Hydrogen gas mass vs. I/v on 2 m gun

Fig. 6

Helium Gas Mass vs. I/v on 2m Gun

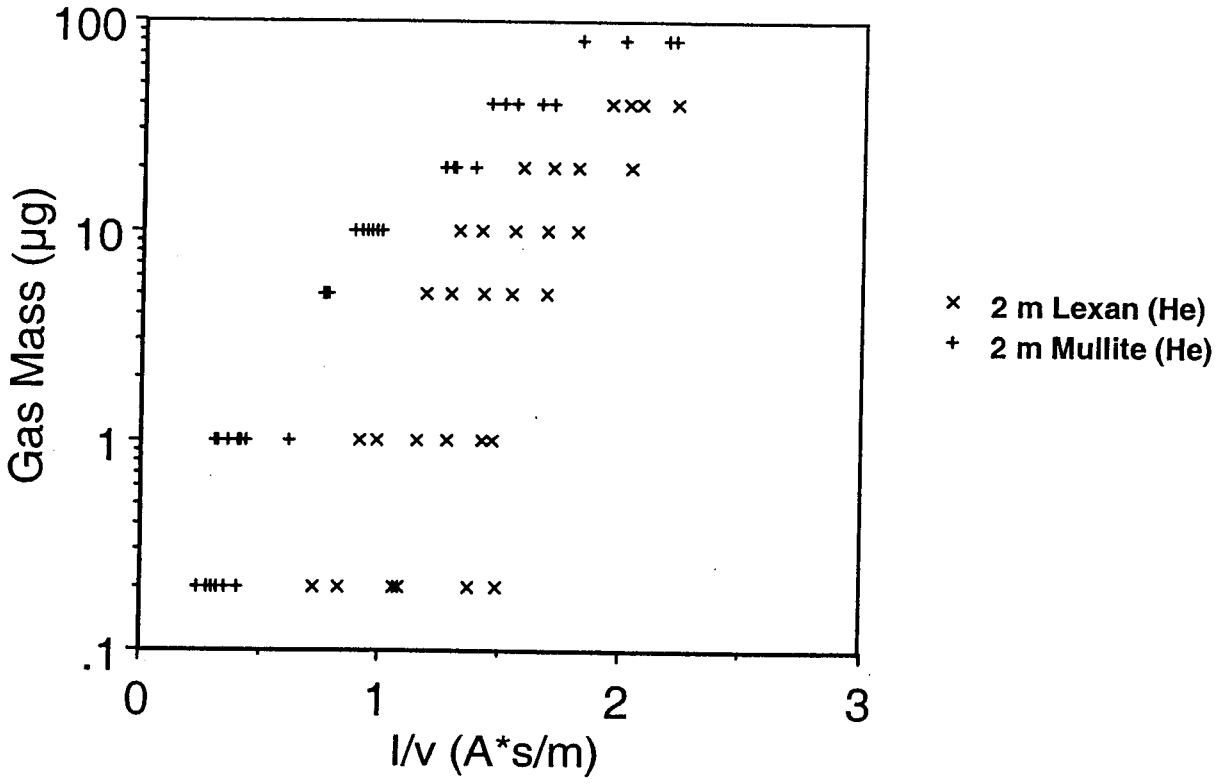

Helium gas mass vs. I/v on 2 m gun

Fig. 7

Comparison of Plasma Spectrum at 3KV and 6KV (10torr)

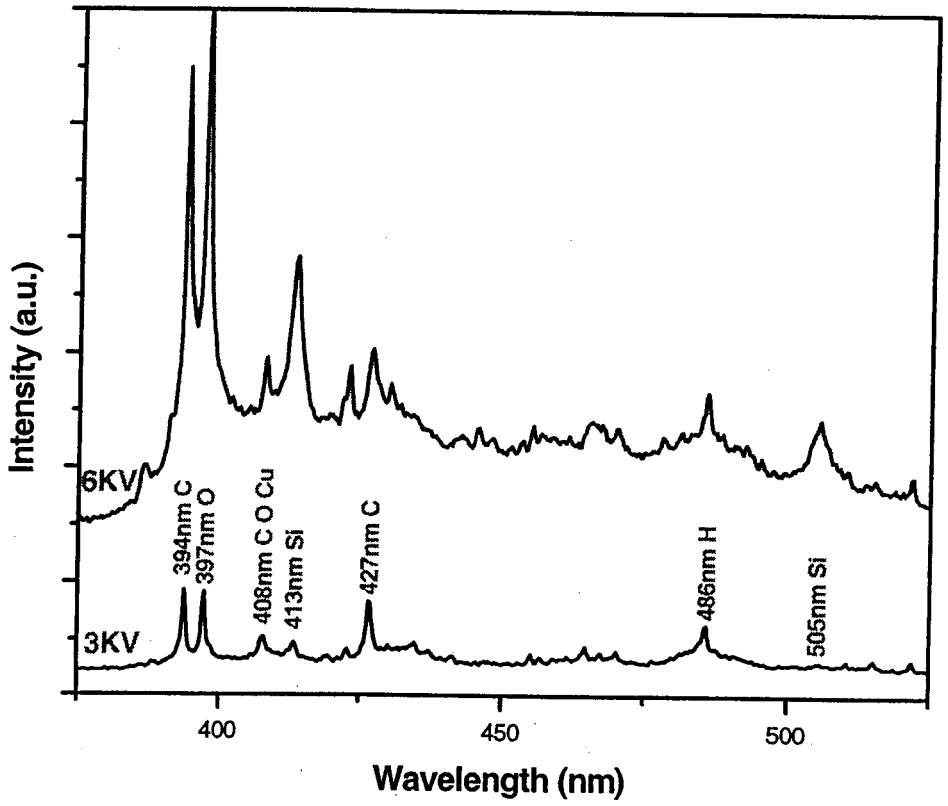

Fig. 8

Intensity of 394nm Impurity Line (C) vs. Bank Voltage at Different Pressures

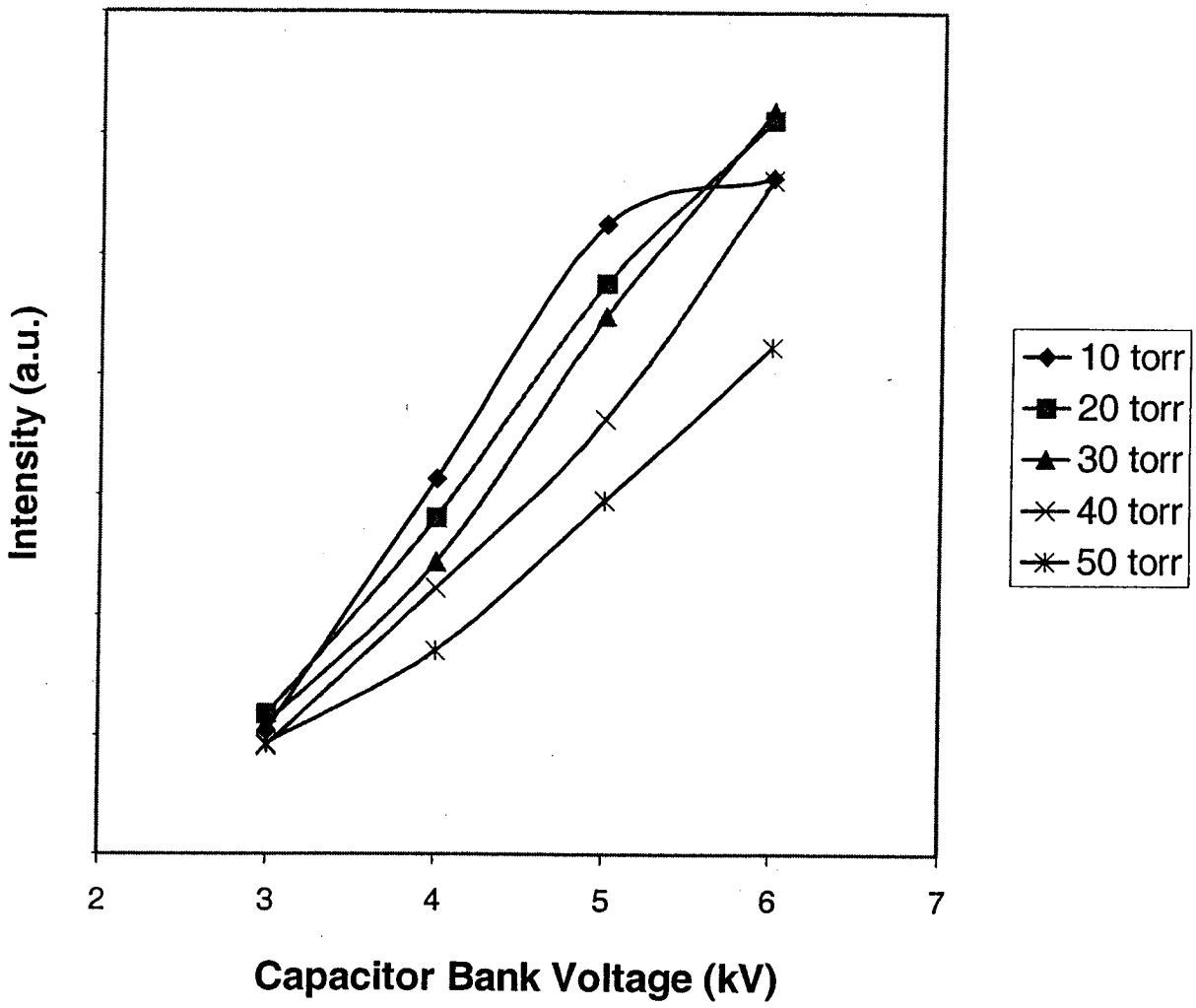

Fig. 9

Intensity of 397nm Impurity Line (O) vs. Bank Voltage at Different Pressures

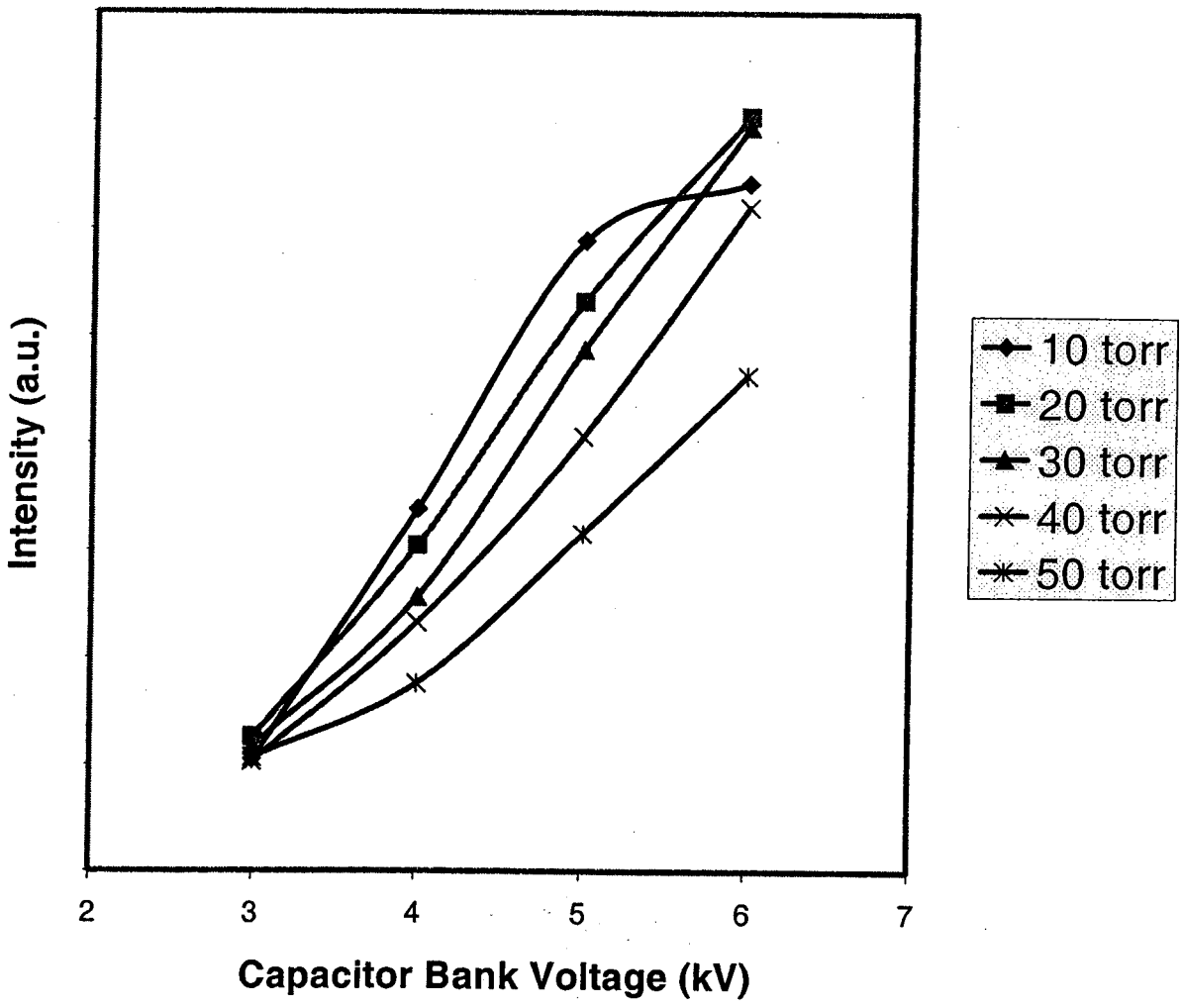

Fig. 10

Intensity of 408nm Impurity Line (C O Cu) vs. Bank Voltage at Different Pressures

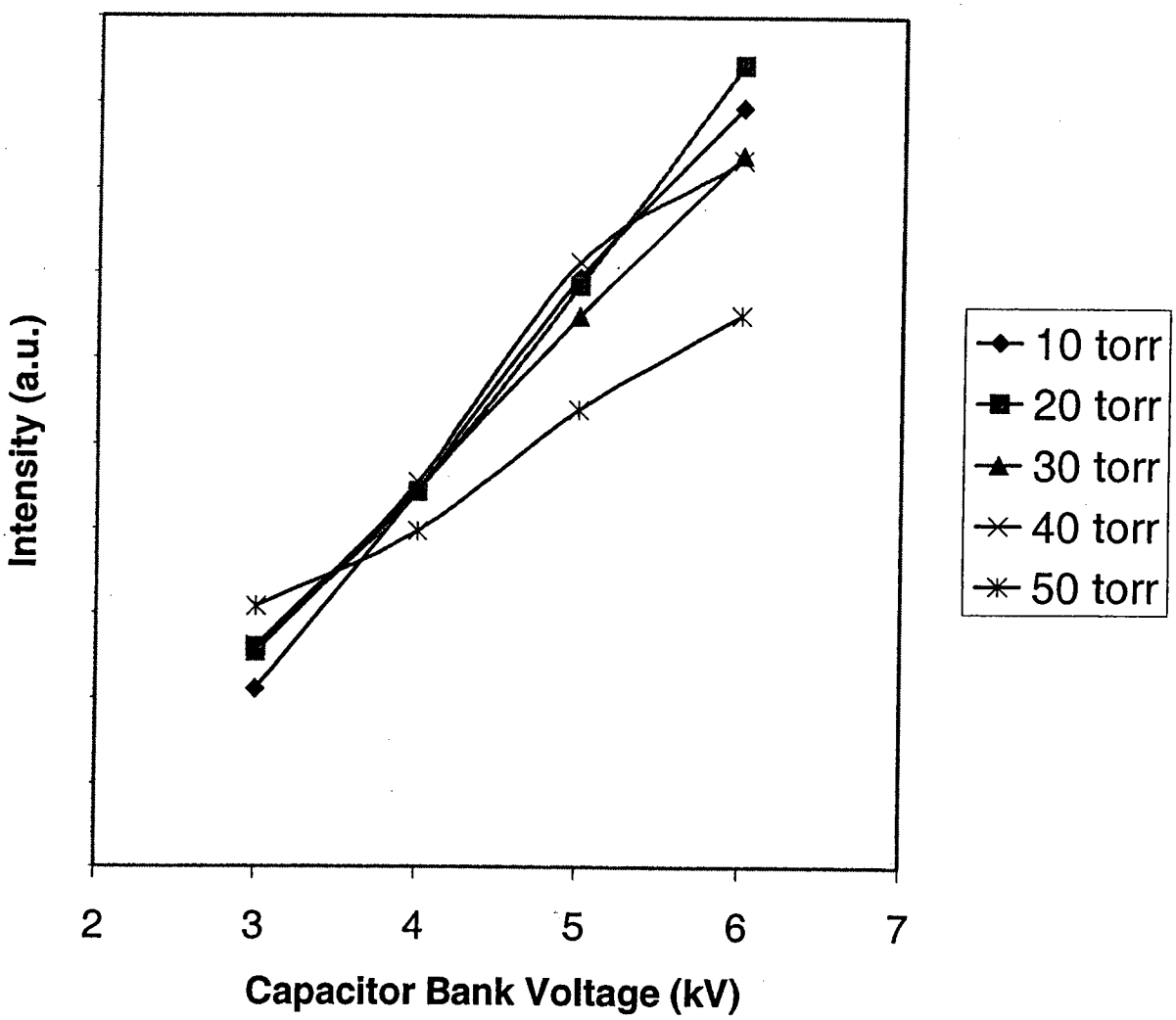

Fig. 11

Intensity of 413nm Impurity Line (Si) vs. Bank Voltage at Different Pressures

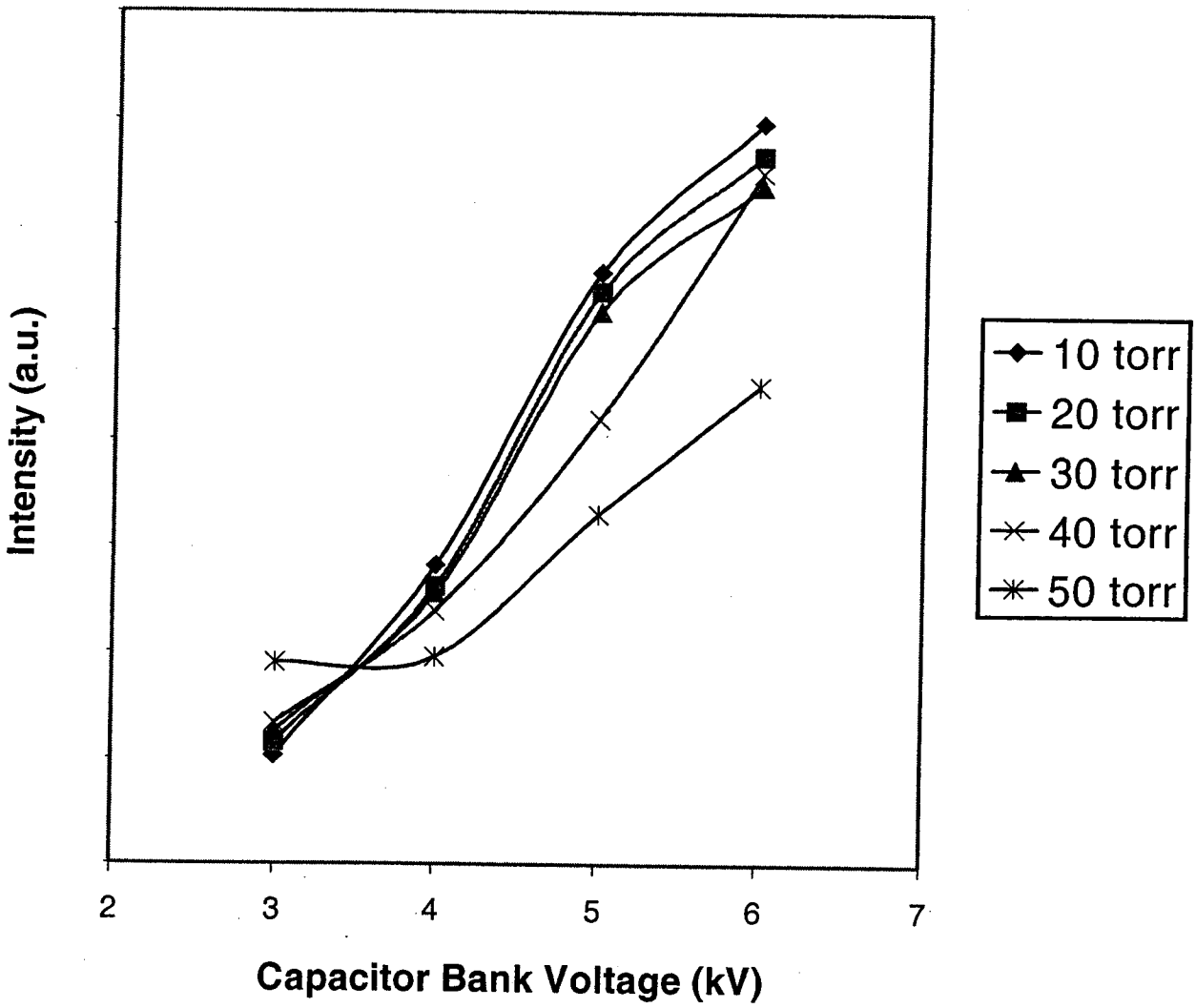

Fig. 12

Intensity of 427nm Impurity Line (C) vs. Bank Voltage at Different Pressures

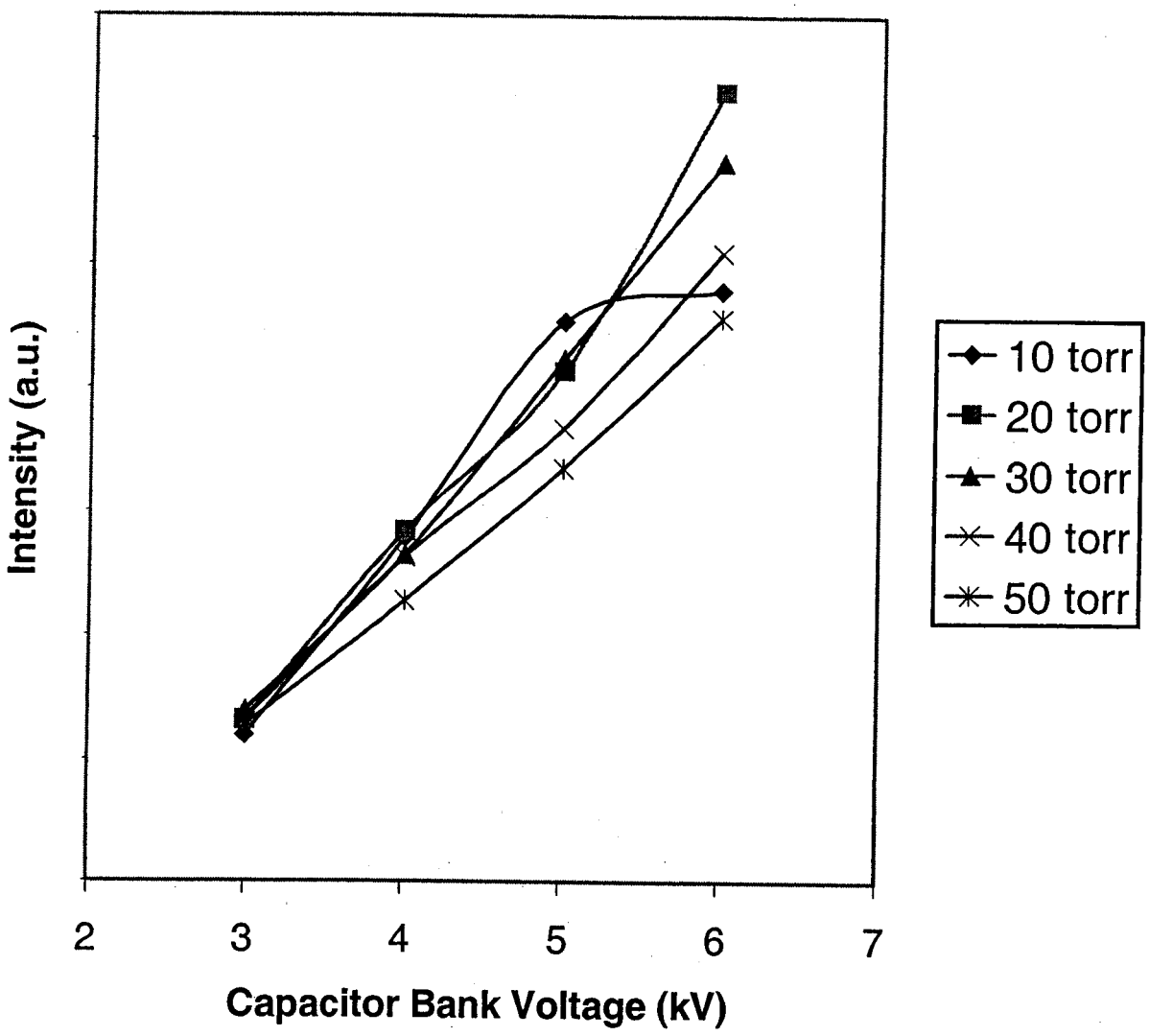

Fig. 13

Comparison of Intensities of Impurity Lines

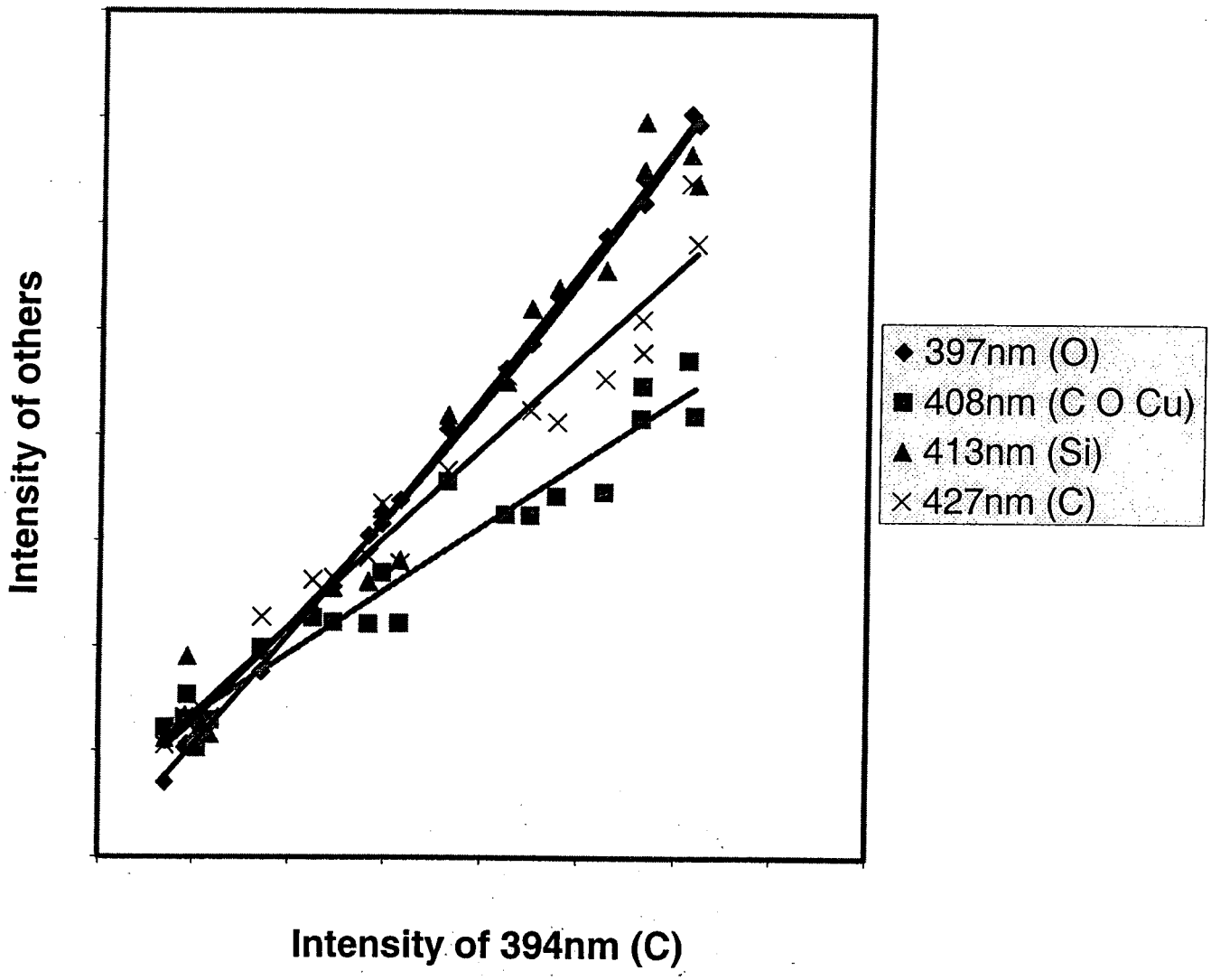

Fig. 14

Transaugmented Railgun

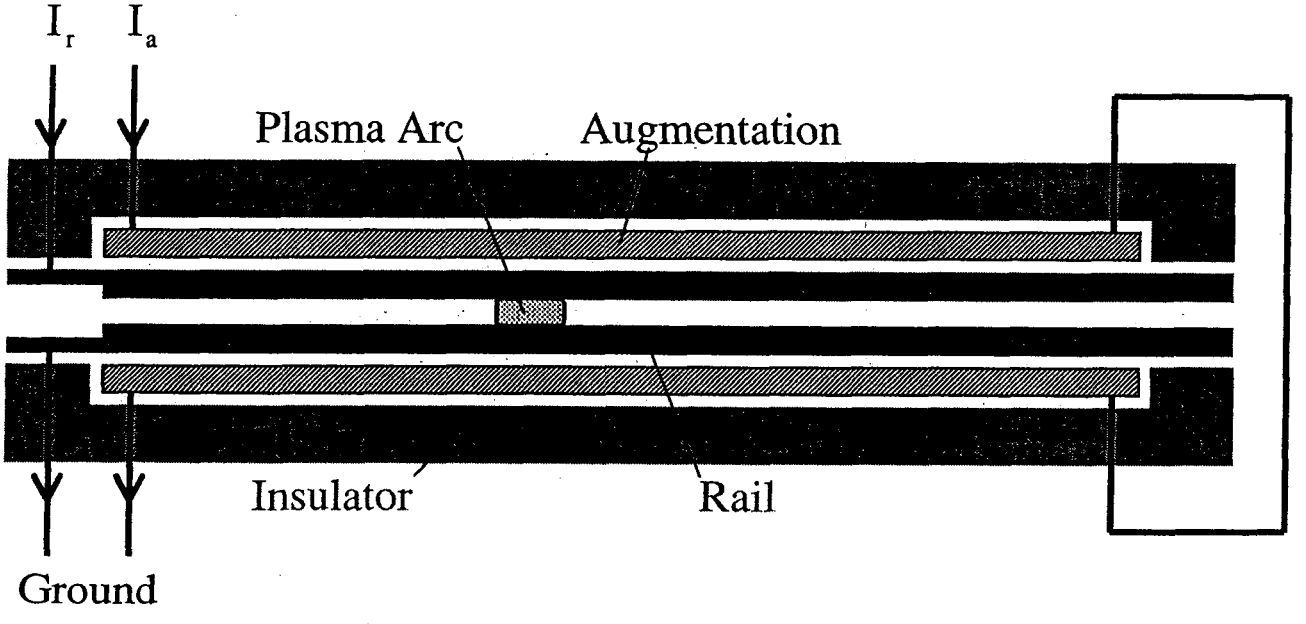

$$F_L = \frac{2\times 9.81\mu_0 r}{\pi} I_r \left(\frac{I_r}{L_r} + \frac{I_a}{L_a} \right)$$

Fig. 15